Vibration Mitigation and Dynamics of a Rotor Equipped with a Multi-stable Nonlinear Vibration Absorber

Ata Rakhshaei[1]

[1]Faculty of Mechanical Engineering, Tabriz University, Tabriz, Iran.
*Corresponding author: atarakhshaye@gmail.com

Abstract

Excessive vibration of the rotor system is one of the main reasons for the failure of rotating machines. Thus, developing cost-effective methods to reduce such vibrations is critical. One effective and practical method for mitigating rotor system vibrations is using a nonlinear vibration absorber (NVA) or nonlinear energy sink (NES). NVA significantly reduces vibration amplitude and prevents resonance in rotor systems. Previous studies have extensively explored vibration reduction in rotor systems using NVA via numerical methods. However, analytical approaches, such as perturbation methods, have not yet been employed. In this paper, due to the many advantages of the analysis, for the first time, the dynamics of rotor system equipped with a multi-stable nonlinear vibration absorber (MNVA) has been investigated using the multiple scales method. The spring stiffness of the vibration absorber has been assumed to be a combination of linear and nonlinear components, and the response has been obtained using a first-order approximation. Then have been examined the impact of various parameters on the system's oscillation amplitude and also the possibility of jump phenomenon. To validate the results, the response obtained from the present analytical method has been compared with the numerical method available in the technical literature. Lastly, the advantages of using MNVA compared to linear vibration absorber (LVA) have been investigated. The results show that the first-order approximation using the multiple scales method provides accurate solutions, closely matching numerical results. The vibration absorption rate of MNVA is 22% higher than that of the LVA.

Keywords: Rotor system, nonlinear vibration absorber, vibration amplitude reduction, jump phenomenon, multiple scales method.

1. Introduction

Vibration is an inherent characteristic of all rotating machinery and must be controlled within acceptable thresholds to ensure reliable and safe operation [1-3]. Deviations from these established standards can result in elevated vibration levels, which may cause severe damage to components, leading to system failure and, in extreme cases, irreversible damage [4, 5]. High-amplitude vibrations typically manifest at certain critical speeds of the rotor, contributing to rotor shaft eccentricity. This excessive vibration may weaken connections and compromise structural integrity, ultimately impairing the functionality of the rotating machinery [6]. Consequently, the

development of effective solutions for mitigating vibrations in rotating systems has become a significant focus of research [7-10].

Vibration absorbers play a pivotal role in mitigating overall vibrations in rotor systems by transferring vibrational energy from the rotor to the absorber. Due to advantages such as low cost, simple structure, and operation without the need for external power sources, they have garnered significant attention in the engineering community [11-14]. The concept of the vibration absorber was first introduced by Watts [15], and the first practical implementation—a mass-spring system attached to the primary device—was proposed by Frahm [16]. Vibration absorbers for rotor systems are generally categorized into passive [17, 18] and semi-active (active) types [19, 20]. Both passive and active vibration absorbers are effective in reducing rotor system vibrations; however, each type has inherent limitations. Passive absorbers are generally restricted to operating within a narrow frequency range near resonance, limiting their effectiveness across broader frequency bands. On the other hand, active vibration absorbers, while capable of adapting to a wider range of frequencies, are complex and costly due to their intricate design and dependence on external energy sources. In contrast, nonlinear vibration absorbers (NVA) or nonlinear energy sinks (NES) [21-24] present a promising alternative. Unlike traditional absorbers, NVAs consist of small masses that do not rotate with the rotor, offering a more versatile and potentially cost-effective solution for vibration mitigation. Consequently, their imbalance does not affect the behavior of the rotor system. These NESs possess multiple equilibrium points and can reduce vibrations over a wide frequency range. NESs have been applied in various industries, including aerospace [25], rotating machinery [26], architecture [27], and other fields. The study of vibration reduction in rotor systems using NES has been ongoing for a long time. For example, Bergeot et al. [28] examined a ground-resonant helicopter model equipped with a cubic absorber. They concluded that the NES plays a critical role in reducing vibrations in rotating machines and that a NES can reduce resonance vibrations in helicopters.

Yao et al. [29] proposed a bi-stable nonlinear energy sink (BNES) made of a buckled beam to absorb vibrations in an unbalanced rotor system. They derived the dynamic equations of a rotor system equipped with the BNES and then numerically studied the transient and steady-state responses. Finally, they conducted experimental tests to validate the effect of the BNES. The numerical and experimental results showed that the designed BNES reduced the vibration of the rotor system by 60% and could absorb a wide range of vibrations. Abu Seer et al. [30] examined a prototype of an electromagnetic torsional vibration absorber designed to control torsional vibrations in rotating machinery. Yao et al. [31] proposed a multi-stable nonlinear energy sink (MNES), combining positive and negative stiffness, to reduce rotor system vibrations. In their design, the negative stiffness was achieved using circular permanent magnets. The results indicated that their proposed MNES effectively reduced rotor system vibrations, and the negative stiffness increased the absorber's operating frequency range. Xiaomin Dong et al. [32] studied the performance of a novel torsional vibration absorber with variable magnetic stiffness and damping, both theoretically and experimentally. The results demonstrated that the torsional vibration absorber efficiently reduced rotor system vibrations. Yao et al. [33] developed a MNES to reduce the vibrations of unbalanced rotor systems. They derived the dynamic equations of the rotor system and, based on them, numerically examined the transient and steady-state responses. Their numerical and experimental results showed that the MNES was capable of reducing vibrations

across a wide range of rotor system imbalances. Cao et al. [34] found that excessive vibration in rotor-blade systems was one of the leading causes of failure in rotating machinery, and therefore, a NES was required. They first introduced the structure of the NES mechanism, then derived the dynamic equations for the rotor-blade system using Lagrangian methods, and finally conducted a simple experiment to test the vibration reduction ability of the NES in a rotor-blade system. Their results showed that, under the given parameters, the absorber performed better in the presence and absence of damping, achieving a vibration absorption rate of 93% in numerical simulations and 88% in experimental tests. Hongliang Yao et al. [35] proposed a vibration absorber for unbalanced rotor systems composed of coil springs and magnets.

Pu Gao et al. [36] studied a new type of electromagnetic torsional vibration absorber with variable stiffness. They first conducted a dynamic simulation with the transient response for the system's mechanical structure, then analyzed the magnetic field parameters, modal analysis, natural frequency, and damping effect of the absorber. Finally, they built a prototype of the electromagnetic torsional vibration absorber. The results showed that the torsional electromagnetic vibration absorber efficiently reduced rotor system vibrations. Hongliang Yao et al. [37] also studied a Ground nonlinear energy sink (GNES) attached to a rotor system with a simple structure. They analyzed the GNES and then derived the dynamic equations of the rotor and GNES systems. First, they performed a numerical simulation to investigate the vibration absorption of the rotor system, then conducted experimental tests on the rotor system to validate the vibration reduction effect. Their results showed that the GNES effectively reduced rotor system vibrations, with the numerical simulation achieving a vibration absorption rate of 78% and the experimental test achieving 68%.

A review of previous research highlights the significant influence of vibration absorbers' dynamic behavior in attenuating rotor system vibrations. Notably, most studies have employed numerical methods, while analytical approaches, such as perturbation analysis, have been largely overlooked. Although numerical methods are efficient and allow for the quick determination of time and frequency responses for specific system parameters, approximate analytical solutions offer distinct advantages. These solutions, while more challenging to derive, are often preferred as they provide deeper insights by predicting system trajectories, analyzing the influence of various parameters, and delivering qualitative assessments of system behavior. The previous work by Yao et al. [37] inspired the authors to further explore the performance of multi-stable nonlinear vibration absorbers (MNVAs), motivating the current study. The primary objectives and innovations of this work are as follows:

1. The spring stiffness of the vibration absorber is modeled as a combination of linear and nonlinear components.
2. For the first time, the response of a rotor system equipped with a MNVA is derived using the method of multiple scales with a first-order approximation. This study investigates the influence of both linear and nonlinear parameters on the oscillation amplitude, as well as the potential occurrence of jump phenomena.
3. To validate the proposed analytical solution, the results obtained via the multiple scales method are compared with the numerical results from Yao et al., and the advantages of MNVA over linear vibration absorbers (LVA) are examined.

The findings of this study offer valuable insights for engineers seeking to reduce or eliminate rotor system vibrations over a wide frequency range through the implementation of MNVAs.

2. Mathematical formulation

In this section, the governing equations of a rotor system equipped with a MNVA, as specified in reference [37], are examined. Initially, it is assumed:

$$k_c(x - x_n) = k_{c0}(x - x_n) - k_{n1}(x - x_n)^3 \tag{1}$$

where k_{c0} and k_{n1} represent the linear and nonlinear stiffness of the vibration absorber's spring in the axial direction. Figure 1 illustrates the dynamic model of a MNVA connected to a rotor system.
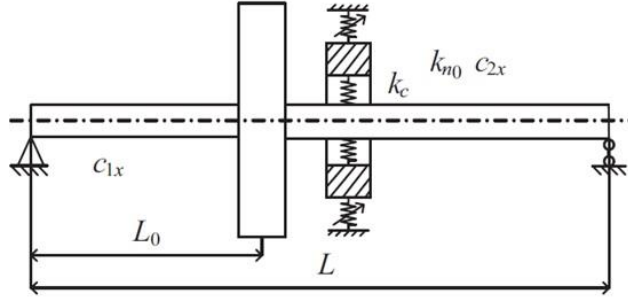
Figure 1: Dynamic model of a rotor system equipped with a MNVA [37].

Thus, the governing equations of motion for the rotor system equipped with a MNVA in the horizontal direction can be formulated as follows:

$$m_1 \ddot{x} + c_{1x} \dot{x} + k_x x + k_{c0}(x - x_n) - k_{n1}(x - x_n)^3 = m_1 r \omega^2 \cos(\omega t)$$

$$m_n \ddot{x}_n + c_{2x} \dot{x}_n - k_{c0}(x - x_n) - k_{n1}(x - x_n)^3 + k_{n0} x_n + k_n x_n^3 = 0 \tag{2}$$

where the primary nonlinear vibration system consists of mass m_1, damping coefficient c_{1x}‹ rotor system stiffness k_x in the axial direction, the rotor shaft eccentricity r, and the rotor's angular velocity ω. To reduce the vibration amplitude of the primary system, a MNVA is used, characterized by mass m_n, damping coefficient c_{2x}, total bending stiffness of the connecting rods k_{n0} and nonlinear stiffness of the connecting rods k_n.

Due to the inherent nonlinearity of the governing equations, the method of multiple time scales is applied to obtain an approximate analytical solution. First, the governing equations (2) are rewritten in their dimensionless form to simplify the analysis. The following dimensionless variables are introduced:

$$\ddot{x} + \varepsilon \mu_{1,x} \dot{x} + \omega_{x,c}^2 x - \varepsilon \alpha x^3 + 3\varepsilon \alpha x^2 x_n - 3\varepsilon \alpha x x_n^2 + \varepsilon \alpha x_n^3 - \varepsilon \beta_c x_n = (\varepsilon f / m_1) \cos(\omega t)$$

$$\ddot{x}_n + \varepsilon \mu_{2,x} \dot{x}_n - \omega_{c,n}^2 x + \omega_{c,n}^2 x_n + \varepsilon \alpha_n x^3 - 3\varepsilon \alpha_n x^2 x_n + 3\varepsilon \alpha_n x x_n^2 - \varepsilon \alpha_n x_n^3 + \omega_{n,0}^2 x_n + \varepsilon \beta_n x_n^3 = 0 \tag{3}$$

where $f = m_1 r \omega^2$ represents the centrifugal force from the center of the rotor system and ε is a small dimensionless perturbation parameter. The remaining parameters are defined as follows:

4

$$\mu_{1,x} = \frac{c_{1x}}{m_1}, \qquad \omega_{x,c}^2 = \frac{k_x + k_{c0}}{m_1}, \qquad \alpha = \frac{k_{n1}}{m_1}, \qquad \beta_c = \frac{k_{c0}}{m_1}$$

$$\mu_{2,x} = \frac{c_{2x}}{m_n}, \qquad \omega_{c,n}^2 = \frac{k_{co}}{m_n}, \qquad \alpha_n = \frac{k_{n1}}{m_n}, \qquad \omega_n^2 = \frac{k_{n0}}{m_n}, \qquad \beta_n = \frac{k_n}{m_n}$$

(4)

It is assumed that the solution to the dimensionless equations (3), considering a first-order approximation of $O(\epsilon)$, takes the following form as proposed in [38]:

$$x(t,\varepsilon) = x_{10}(T_0,T_1) + \varepsilon x_{11}(T_0,T_1) + \dots$$

(5)

$$x_n(t,\varepsilon) = x_{n0}(T_0,T_1) + \varepsilon x_{n1}(T_0,T_1) + \dots$$

where temporal scales are defined as follows:

$$T_n = \varepsilon^n T, \qquad n = 0,1,2,\dots$$

(6)

Therefore, $T_0 = t$ and $T_1 = \varepsilon t$ represent the fast and slow time scales, respectively. The first and higher-order derivatives with respect to time could be expanded as partial derivatives with respect to T_0 and T_1 as follows:

$$\frac{d}{dt} = \frac{dT_0}{dt}\frac{\partial}{\partial T_0} + \frac{dT_1}{dt}\frac{\partial}{\partial T_1} = D_0 + \varepsilon D_1 + O(\varepsilon^2) \quad , \qquad \frac{d^2}{dt^2} = \frac{\partial^2}{\partial T_0^2} + 2\varepsilon\frac{\partial^2}{\partial T_0 \partial T_1} = D_0^2 + 2\varepsilon D_0 D_1 + O(\varepsilon^2)$$ (7)

where

$$D_n = \frac{\partial}{\partial T_n}, \qquad n = 0,1,2,\dots$$

(8)

By substituting the assumed solutions from equations (5) and (7) into the original equations of motion (3), and collecting terms of the same order of ϵ\epsilon$\epsilon$, the governing equations are expressed as follows:

$$(D_0^2 + 2\varepsilon D_0 D_1)(x_{10} + \varepsilon x_{11}) + \varepsilon\mu_{1,x}\big((D_0 + \varepsilon D_1)(x_{10} + \varepsilon x_{11})\big) + \omega_{x,c}^2(x_{10} + \varepsilon x_{11})$$
$$- \varepsilon\alpha(x_{10} + \varepsilon x_{11})^3 + 3\varepsilon\alpha(x_{10} + \varepsilon x_{11})^2(x_{n0} + \varepsilon_{n1}) - 3\varepsilon\alpha(x_{10} + \varepsilon x_{11})(x_{n0} + \varepsilon x_{n1})^2$$

(9)

$$+ \varepsilon\alpha(x_{n0} + \varepsilon x_{n1})^3 - \varepsilon\beta_c(x_{n0} + \varepsilon x_{n1}) = \frac{\varepsilon f}{m_1}\cos(\omega_s t)$$

$$(D_0^2 + 2\varepsilon D_0 D_1)(x_{n0} + \varepsilon x_{n1}) + \varepsilon\mu_{2,x}\big((D_0 + \varepsilon D_1)(x_{n0} + \varepsilon x_{n1})\big) - \omega_{c,n}^2(x_{10} + \varepsilon x_{11})$$
$$+ \omega_{c,n}^2(x_{n0} + \varepsilon x_{n1}) + \varepsilon\alpha_n(x_{10} + \varepsilon x_{11})^3 - 3\varepsilon\alpha_n(x_{10} + \varepsilon x_{11})^2(x_{n0} + \varepsilon_{n1})$$
$$+ 3\varepsilon\alpha_n(x_{10} + \varepsilon x_{11})(x_{n0} + \varepsilon x_{n1})^2 - \varepsilon\alpha_n(x_{n0} + \varepsilon x_{n1})^3 + \omega_{n,0}^2(x_{n0} + \varepsilon x_{n1})$$
$$+ \varepsilon\beta_n(x_{n0} + \varepsilon x_{n1})^3 = 0$$

(10)

By equating the coefficients of terms with equal powers of ϵ, we derive separate equations for each order of approximation. For the zeroth-order terms $O(1)$ and the first-order terms $O(\epsilon)$, we obtain the following governing equations:

$$\varepsilon^0: \qquad D_0^2 x_{10} + \omega_{x,c}^2 x_{10} = 0$$

(11)

$$D_0^2 x_{n0} + \omega_{n,0}^2 x_{n0} = \omega_{c,n}^2 x_{10}$$

(12)

$$\varepsilon^1: \quad D_0^2 x_{11} + \omega_{x,c}^2 x_{11} = \alpha x_{10}^3 - 3\alpha x_{10}^2 x_{n0} + 3\alpha x_{10} x_{n0}^2 - \alpha x_{n0}^3 + \beta_c x_{n0}$$
$$- \mu_{1,x} D_0 x_{10} - 2 D_0 D_1 x_{10} + \frac{\varepsilon f}{m_1} \cos(\omega_s t) \tag{13}$$

$$D_0^2 x_{n1} + (\omega_{c,n}^2 + \omega_{n,0}^2) x_{n1} = -\alpha_n x_{10}^3 + 3\alpha_n x_{10}^2 x_{n0} - 3\alpha_n x_{10} x_{n0}^2 + \alpha_n x_{n0}^3$$
$$- \beta_n x_{n0}^3 + \omega_{c,n}^2 x_{11} - \mu_{2,x} D_0 x_{n0} - 2 D_0 D_1 x_{n0} \tag{14}$$

The general solution for equation (11) is:

$$x_{10} = A(T_1) \exp(i\omega_{x,c} T_0) + \overline{A(T_1)} \exp(-i\omega_{x,c} T_0) \tag{15}$$

where A is a function of T_1 and $\overline{A}$ is the complex conjugate of A. Substituting the answer to x_{10} into equation (12), the solution of x_{n0} is obtained as:

$$x_{n0} = B(T_1) \exp(i\sqrt{\omega_{c,n}^2 + \omega_{n,0}^2} T_0) + \overline{B(T_1)} \exp(-i\sqrt{\omega_{c,n}^2 + \omega_{n,0}^2} T_0)$$
$$+ F_0 A(T_1) \exp(i\omega_{x,c} T_0) + F_0 \overline{A(T_1)} \exp(-i\omega_{x,c} T_0) \tag{16}$$

where $F_0 = \dfrac{\omega_{c,n}^2}{\omega_{c,n}^2 + \omega_{n,0}^2 - \omega_{x,c}^2}$ and B are also a function T_1.

For the primary resonance, it is assumed that the excitation frequency is approximately equal to the natural frequency of the primary system:

$$\omega = \omega_{x,c} + \varepsilon\sigma \tag{17}$$

where σ is a tuning parameter representing the proximity of ω and $\omega_{x,c}$. By substituting equations (15), (16), and (17) into equations (13) and (14), we get:

$$D_0^2 x_{11} + \omega_{x,c}^2 x_{11} = (-\alpha F_0^3 A^3 + 3\alpha F_0^2 A^3 - 3\alpha F_0 A^3 + \alpha A^3) \exp(i3\omega_{x,c} T_0) + (-3\alpha F_0^2 A^2 B$$
$$+ 6\alpha F_0 A^2 B - 3\alpha A^2 B) \exp(i\sqrt{\omega_{c,n}^2 + \omega_{n,0}^2} T_0 + i2\omega_{x,c} T_0) + ((-3\alpha F_0 AB^2$$
$$+ 3\alpha AB^2) \exp(i2\sqrt{\omega_{c,n}^2 + \omega_{n,0}^2} T_0) + \frac{1}{2} \frac{f}{m_1} \exp(i\sigma T_1) + 3\alpha A^2 \overline{A}$$
$$- i\mu_{1,x}\omega_{x,c} A - 6\alpha F_0 AB\overline{B} + 9\alpha F_0^2 A^2 \overline{A} + 6\alpha AB\overline{B} - 9\alpha F_0 A^2 \overline{A} - 3\alpha F_0^3 A^2 \overline{A}$$
$$- i2\omega_{x,c}(D_1 A) + F_0 \beta_c A) \exp(i\omega_{x,c} T_0) + (-\alpha B^3) \exp(i3\sqrt{\omega_{c,n}^2 + \omega_{n,0}^2} T_0)$$
$$+ (-6\alpha F_0^2 A\overline{A}B + 12\alpha F_0 A\overline{A}B - 6\alpha A\overline{A}B - 3\alpha B^2 \overline{B} + \beta_c B) \exp(i\sqrt{\omega_{c,n}^2 + \omega_{n,0}^2} T_0) + CC \tag{18}$$

$$D_0^2 x_{n1} + (\omega_{c,n}^2 + \omega_{n,0}^2)x_{n1} = (3\alpha_n F_0^3 A^2\overline{A} - 3\beta_n F_0^3 A^2\overline{A} - 9\alpha_n F_0^2 A^2\overline{A} + 9\alpha_n F_0 A^2\overline{A} + 6\alpha_n F_0 AB\overline{B}$$
$$- 6\beta_n F_0 AB\overline{B} - i\mu_{2,x}\omega_{x,c}F_0 A - i2\omega_{x,c}F_0(D_1 A) - 3\alpha_n A^2\overline{A}$$
$$- 6\alpha_n AB\overline{B})\exp(i\omega_{x,c}T_0) + (\alpha_n F_0^3 A^3 - \beta_n F_0^3 A^3 - 3\alpha_n F_0^2 A^3 + 3\alpha_n F_0 A^3$$
$$- \alpha_n A^3)\exp(i3\omega_{x,c}T_0) + (6\alpha_n F_0^2 A\overline{A}B - 6\beta_n F_0^2 A\overline{A}B - 12\alpha_n F_0 A\overline{A}B$$
$$+ 6\alpha_n A\overline{A}B - i\mu_{2,x}\sqrt{\omega_{c,n}^2 + \omega_{n,0}^2}B + 3\alpha_n B^2\overline{B} - 3\beta_n B^2\overline{B}$$
$$- i2\sqrt{\omega_{c,n}^2 + \omega_{n,0}^2}(D_1 B))\exp(i\sqrt{\omega_{c,n}^2 + \omega_{n,0}^2}T_0) + (\alpha_n B^3$$
$$- \beta_n B^3)\exp(i3\sqrt{\omega_{c,n}^2 + \omega_{n,0}^2}T_0) + (3\alpha_n F_0^2 A^2 B - 3\beta_n F_0^2 A^2 B - 6\alpha_n F_0 A^2 B$$
$$+ 3\alpha_n A^2 B)\exp(i\sqrt{\omega_{c,n}^2 + \omega_{n,0}^2}T_0 + i2\omega_{x,c}T_0) + (3\alpha_n F_0 AB^2 - 3\beta_n F_0 AB^2$$
$$- 3\alpha_n AB^2)\exp(i2\sqrt{\omega_{c,n}^2 + \omega_{n,0}^2}T_0 + i\omega_{x,c}T_0) + \omega_{c,n}^2 x_{11} + CC \tag{19}$$

In both equations (18) and (19), the terms $\overline{A}(T_1)$ and $\overline{B}(T_1)$ represent the complex conjugates of $A(T_1)$ and $B(T_1)$. To simplify, these are shown as $\overline{A}$, A, $\overline{B}$, and B. CC represents the complex conjugate of the former terms.

To obtain the solution for x_{n1}, we first solve for x_{11} and substitute it into equation (19). Thus, we first need to extract the terms with a coefficient of $i\sqrt{\omega_{c,n}^2 + \omega_{n,0}^2}T_0$ from equation (18) and place them on the left-hand side of the equation. Having solved and simplified, the solution of x_{11} can be written as below:

$$x_{11} = KB\exp(i\sqrt{\omega_{c,n}^2 + \omega_{n,0}^2}T_0) + cc \tag{20}$$

where $K = \dfrac{(-6\alpha F_0^2 A\overline{A} + 12\alpha F_0 A\overline{A} - 6\alpha A\overline{A} - 3\alpha B\overline{B} + \beta_c)}{\omega_{x,c}^2 - (\omega_{c,n}^2 + \omega_{n,0}^2)}$. Therefore, the secular terms in equations (18) and (19) are:

$$\frac{1}{2}\frac{f}{m_1}\exp(i\sigma T_1) + 3\alpha A^2\overline{A} - i\mu_{1,x}\omega_{x,c}A - 6\alpha F_0 AB\overline{B} + 9\alpha F_0^2 A^2\overline{A} + 6\alpha AB\overline{B}$$
$$-9\alpha F_0 A^2\overline{A} - 3\alpha F_0^3 A^2\overline{A} - i2\omega_{x,c}(D_1 A) + F_0\beta_c A = 0 \tag{21}$$

$$6\alpha_n F_0^2 A\overline{A}B - 6\beta_n F_0^2 A\overline{A}B - 12\alpha_n F_0 A\overline{A}B + 6\alpha_n A\overline{A}B - i\mu_{2,x}\sqrt{\omega_{c,n}^2 + \omega_{n,0}^2}B$$
$$+3\alpha_n B^2\overline{B} - 3\beta_n B^2\overline{B} - i2\sqrt{\omega_{c,n}^2 + \omega_{n,0}^2}(D_1 B) + K\omega_{c,n}^2 B = 0 \tag{22}$$

The functions A and B ($A(T_1)$ and $B(T_1)$) are expressed in polar form as follows:

$$A = \frac{1}{2}a(T_1)\exp[i\beta(T_1)], \qquad B = \frac{1}{2}b(T_1)\exp[i\theta(T_1)] \tag{23}$$

where $a(T_1)$, $b(T_1)$, $\beta(T_1)$, and $\theta(T_1)$ are functions of T_1.

By substituting equation (23) into equations (21) and (22), and then separating the real and imaginary parts, we obtain the following equations:

$$\dot{a} = g_{11}a - e\sin(\gamma)$$
$$a\dot{\gamma} = g_{22}a^3 + (-g_{210}b^2 - g_{310} - \sigma)a - e\cos(\gamma)$$
$$\dot{b} = h_{11}b \tag{24}$$
$$\frac{3}{4}\frac{\alpha_n F_0 a^2 b}{\sqrt{\omega_{c,n}^2 + \omega_{n,0}^2}} = h_{21}b$$

where $\gamma = \beta - \sigma T_1$, $g_{11} = -\frac{1}{2}\mu_{1,x}$, $e = \frac{1}{2}\frac{f}{m_1\omega_{x,c}}$, $g_{22} = \frac{3}{8}\frac{\alpha F_0^3}{\omega_{x,c}} - \frac{9}{8}\frac{\alpha F_0^2}{\omega_{x,c}} + \frac{9}{8}\frac{\alpha F_0}{\omega_{x,c}} - \frac{3}{8}\frac{\alpha}{\omega_{x,c}}$, $g_{210} = -\frac{3}{4}\frac{\alpha F_0}{\omega_{x,c}} + \frac{3}{4}\frac{\alpha}{\omega_{x,c}}$,

$g_{310} = \frac{1}{2}\frac{F_0\beta_c}{\omega_{x,c}}$, $h_{11} = -\frac{1}{2}\mu_{2,x}$, and $h_{21} = \frac{3}{4}\frac{a^2 F_0\alpha_n}{\sqrt{\omega_{c,n}^2 + \omega_{n,0}^2}}$.

The steady-state response of the system is obtained by substituting $\dot{a} = \dot{b} = 0$ and $\dot{\gamma} = 0$ into equations (24). Therefore, inserting equations (24) into the expression $\sin^2\gamma + \cos^2\gamma = 1$, the steady-state response is given as:

$$g_{11}^2 a^2 + (-\sigma - g_{310} + g_{22}a^2)^2 a^2 = e^2 \tag{25}$$

3. Results and Discussions

This section investigates the influence of both linear and nonlinear parameters of the rotor system equipped with a multi-stable nonlinear vibration absorber (MNVA) on the system's oscillation amplitude, as well as the occurrence of the jump phenomenon or the three-response region. The analysis utilizes the multiple scales method to obtain an approximate analytical solution, which is subsequently compared with numerical solutions obtained via the Runge-Kutta method, as presented in reference [37]. The comparison serves to validate the accuracy of the analytical approach. Additionally, the advantages of employing a MNVA over a traditional linear vibration absorber (LVA) are thoroughly examined, focusing on vibration reduction efficiency and broader operational frequency ranges. The parameter values for the MNVA connected to the rotor system, which are adopted from reference [37], are provided in Table 1. These parameters form the basis for the numerical and analytical analyses conducted in this study. These parameters are essential in the modeling and analysis of the rotor system's dynamic response when equipped with a MNVA. They are employed in both the analytical method of multiple scales and the numerical simulations based on the Runge-Kutta method for a comprehensive comparison of the results.

Table 1. The values of rotor system and MNVA parameters [37]

Rotor System Parameters	Values	MNVA Parameters	Values
m_1	1 (kg)	m_n	0.0813 (kg)
c_{1x}	10 N.s/m	c_{2x}	1.62 N.s/m
k_x	7.6×10^4 (N/m)	k_{c0}	4000 (N/m)
r	3×10^{-5} (m)	k_{n0}	1257.72 (N/m)
ω	251 (rad/s)	k_n	11×10^9 (N/m)

Figure 2 illustrates the impact of the nonlinear stiffness k_{nl} of the vibration absorber's spring on the frequency response of the rotor system equipped with a MNVA. As demonstrated, an increase in k_{nl} from zero results in the frequency response curve bending to the left, signifying a softening spring behavior. Conversely, when k_{nl} decreases from zero, the frequency response curve bends to the right, indicating a stiffening spring effect. In both positive and negative cases of nonlinear stiffness, a three-response region or jumping phenomenon is observed. This jump phenomenon is characteristic of nonlinear systems and reflects the presence of multiple stable and unstable response branches. For values of k_{nl} close to zero, the deviation from the linear frequency response is minimal, and the system exhibits behavior similar to that of a linear system. Furthermore, the maximum oscillation amplitude remains unaffected by variations in k_{nl}, indicating that the nonlinear stiffness primarily influences the system's frequency response shape without altering the peak amplitude.
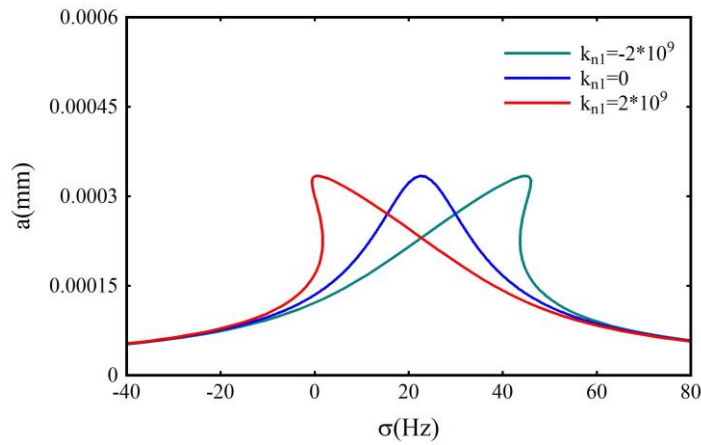
Figure 2: Effect of the nonlinear stiffness of the vibration absorber spring on the frequency response of the rotor system equipped with a MNVA

Figure 3 presents the frequency response curve of the rotor system equipped with a MNVA at three different levels of the damping coefficient c_{1x}. As shown in the figure, an increase in the rotor system's damping leads to a reduction in the system's maximum oscillation amplitude. This behavior is consistent with the expected effects of increased damping, where higher damping levels effectively dissipate more energy from the system, thereby suppressing the vibration amplitude. The diagram clearly demonstrates that as the damping coefficient c_{1x} increases, the peak amplitude decreases, resulting in a smoother and more controlled response. This finding highlights the important role that damping plays in managing the vibrational behavior of rotor systems equipped with nonlinear vibration absorbers, providing a means of improving system stability and reducing excessive vibrations.
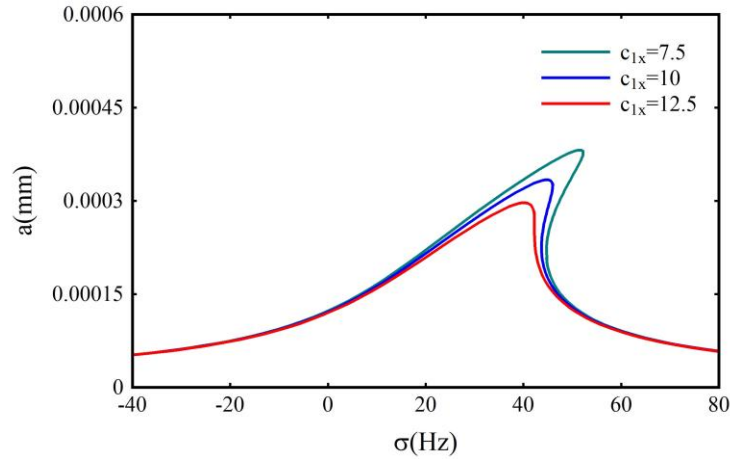
Figure 3: Effect of rotor system damping on the frequency response of the rotor system equipped with a MNVA

Figure 4 illustrates the effect of varying the damping value of the MNVA on the oscillation amplitude of the rotor system equipped with the absorber. As depicted, changes in the absorber's damping value c_{2x} do not significantly influence the system's oscillation amplitude. This behavior can be explained by the parameters defined in the frequency response equation, where the coefficients associated with the absorber's damping term are notably small and approach zero. As a result, even with variations in c_{2x}, the system's response curve remains essentially unchanged, indicating that the damping of the MNVA has a negligible effect on the overall vibration amplitude of the rotor system. This suggests that the system's behavior is more sensitive to other factors, such as nonlinear stiffness, rather than the absorber's damping characteristics.
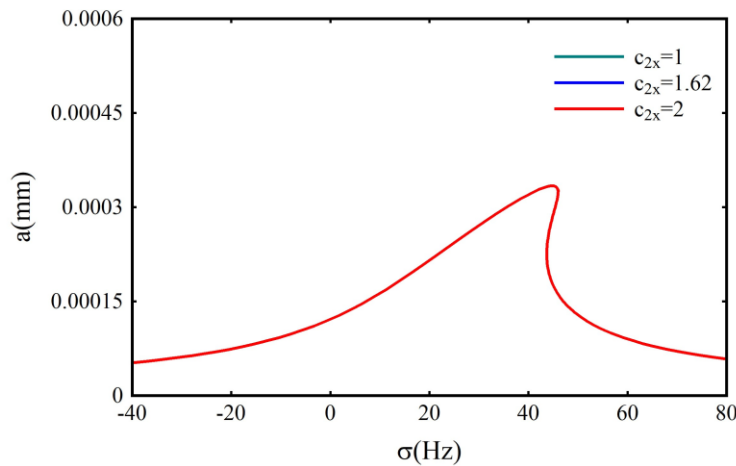
Figure 4: Effect of damping in the MNVA on the frequency response of the rotor system equipped with MNVA

Figure 5 illustrates the variation in oscillation amplitude of the rotor system equipped with a MNVA for different values of the linear stiffness of both the rotor system (k_x) and the MNVA (k_{c0}). As seen in the figure, increasing the stiffness of both the rotor system and the vibration absorber leads to a reduction in the maximum oscillation amplitude. This reduction is accompanied by a noticeable leftward shift in the frequency response curve, indicating that the system begins to exhibit more linear behavior as stiffness increases. Furthermore, as the values of k_x and k_{c0} increase,

the system's frequency response curve continues to shift leftwards and approaches the resonance state. This shift reflects the stiffening effect in the system, where higher stiffness values bring the system closer to its natural frequency, thereby influencing the overall vibration characteristics. This trend suggests that increased stiffness enhances the system's stability by reducing amplitude and modifying the frequency response towards more predictable linear behavior.
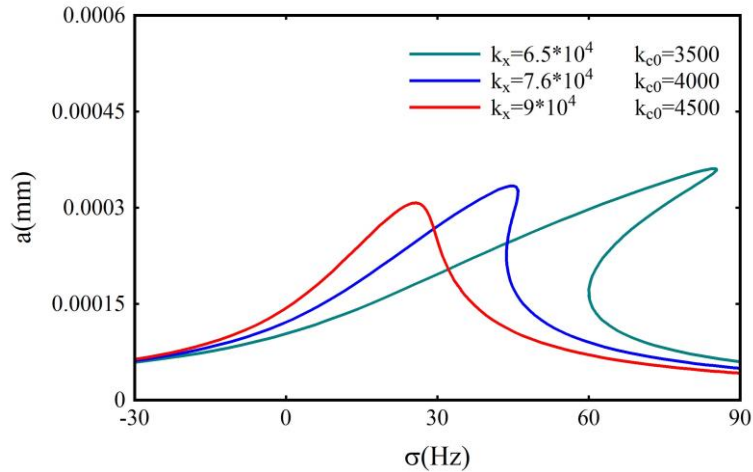
Figure 5: Effect of rotor system stiffness and absorber stiffness on the frequency response of the rotor system equipped with a MNVA

Figure 6 demonstrates the influence of changes in the total bending stiffness (k_{n0}) of the connecting rods of the MNVA on the system's frequency response. As depicted in the diagram, an increase in k_{n0} causes the response curve to shift to the right, moving further away from the resonance state. This behavior indicates that higher stiffness values increase the system's resistance to vibrations, thereby reducing the likelihood of resonance. Additionally, as k_{n0} increases, the frequency response curve exhibits a greater deviation to the right, which results in the formation of a three-response region. This region reflects the occurrence of multiple stable and unstable responses, characteristic of nonlinear systems. The presence of these unstable responses suggests that the system becomes more prone to sudden jumps or bifurcations in its dynamic behavior as the stiffness increases. As σ increases, the amplitude a initially rises, reaches a peak, and then exhibits a decline, suggesting a resonance-like behavior. Each curve shows distinct resonance peaks at different frequencies, indicating how the system's response varies with the parameter k_{n0}.

The figure illustrates the response of a system with varying parameters, specifically highlighting the curves corresponding to different values of k_{n0}. For the green curve ($k_{n0}=1000$), the peak amplitude is approximately 0.00058 mm at around 40 Hz, representing a 287% increase from a baseline of 0.00015 mm. The blue curve ($k_{n0}=1257.72$) reaches the highest peak amplitude of about 0.0006 mm at approximately 50 Hz, marking a 300% increase from the baseline. Conversely, the red curve ($k_{n0}=1500$) shows a peak amplitude of approximately 0.00055 mm at around 60 Hz, reflecting a 267% increase. This analysis reveals that as k_{n0} increases, both the frequency of the peak response shifts to higher values and the amplitudes vary, underscoring the

significant influence of the parameter on the system's dynamic behavior and resonance characteristics.
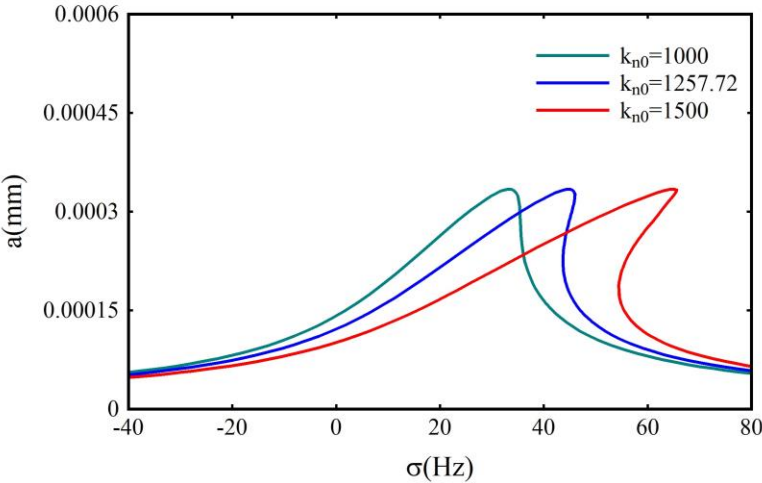
Figure 6: Effect of the total bending stiffness of the connecting rods in the MNVA on the rotor system's frequency response equipped with MNVA

Figure 7 demonstrates the effect of amplitude changes as a function of the tuning parameter for different values of the force factor (f). The graph shows curves for f =1.25, f=1.9, and f=2.5, indicating that as f increases, the oscillation amplitude of the rotor system equipped with a MNVA also increases. Specifically, for f=1.25, the maximum amplitude is approximately 0.0004 mm, while for f=2.5, the amplitude increases by about 100%, reaching 0.0008 mm. Additionally, the frequency response curve shifts to the right as f increases, suggesting that the system's behavior becomes increasingly nonlinear with the rising centrifugal force of the rotor. This shift indicates that higher force factors lead to larger amplitude responses and greater deviation from linearity.
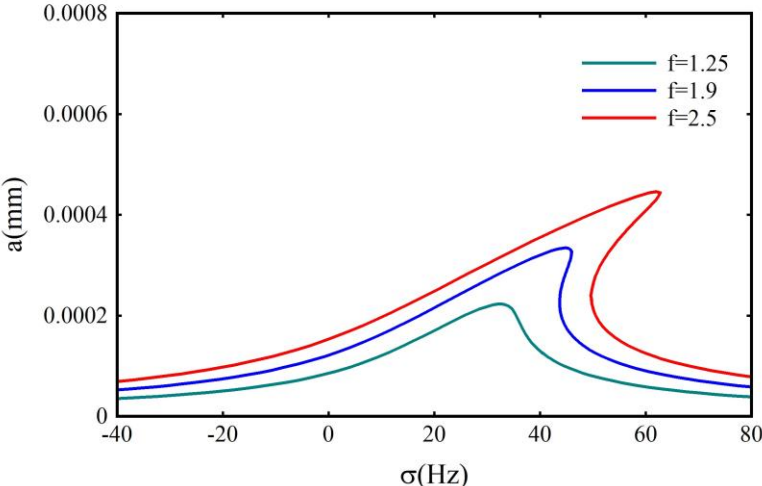
Figure 7: Effect of the rotor system's centrifugal force on the frequency response of the rotor system equipped with MNVA

Initially, assuming $k_{n1} = -5 \times 10^9$ and $f = 1.25$, the jumping phenomenon is examined. According to Figure 8, as σ increases, the amplitude of the rotor system equipped with a non-linear vibration absorber increases from point a to points b and c. From point c, as σ increases, the amplitude suddenly decreases and jumps to point d, which is referred to as the jumping phenomenon. Additionally, reducing σ from point e causes the system amplitude to drop to point d and ultimately to point g. At point g, with a decrease in σ, a jump to point b occurs, resulting in a sudden increase in amplitude. A close inspection of the graph reveals that there are three amplitudes for $b < \sigma < d$. The section of the graph labeled $c - g$ represents an unstable state for the system, and the amplitude never resides in this section of the graph. Depending on the system's initial conditions, the amplitude will settle at one of the higher or lower values corresponding to these values of σ.
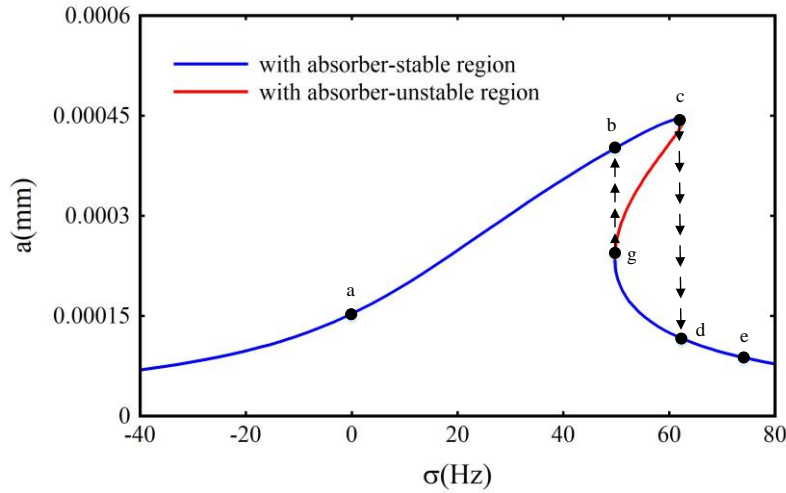
Figure 8: Three-response region or jump phenomenon in the frequency response curve of the rotor system equipped with a MNVA during resonance ($\omega = \omega_{x,c} + \varepsilon\sigma$)

To validate the proposed solution for equations (2) and (3), equation (26) can be expressed as follows:

$$\dot{a} = -\frac{1}{2}\mu_{1,x}a - e\sin(\gamma)$$

(26)

$$a\dot{\gamma} = (\frac{3}{8}\frac{\alpha F_0^3}{\omega_{x,c}} - \frac{9}{8}\frac{\alpha F_0^2}{\omega_{x,c}} + \frac{9}{8}\frac{\alpha F_0}{\omega_{x,c}} - \frac{3}{8}\frac{\alpha}{\omega_{x,c}})a^3 + ((\frac{3}{4}\frac{\alpha F_0}{\omega_{x,c}} + \frac{3}{4}\frac{\alpha}{\omega_{x,c}})b^2 - (\frac{1}{2}\frac{F_0\beta_c}{\omega_{x,c}}) - \sigma)a - e\cos(\gamma)$$

Integrating the two equations in relation (26) and substituting them into $x = a\cos(\omega T_0 - \gamma)$ with initial conditions of $a_0 = 0.4$ and $\gamma_0 = 0.4$ yields the solution to the equation of motion as follows:

$$x = (0.0004242 + 0.4e^{-10t})\cos(282.8427t - 1.2695\ln(e^{-10t}) - \ln(5 \times 10^{10}e^{-10t} + 2.6576 \times 10^8))$$

(27)

where $T_0 = t$, $T_1 = \varepsilon t$, $\varepsilon = 0.01$, and $k_{n1} = 0$.

To evaluate the accuracy of the solution and compare the analytical multiple time scales method with the numerical Runge-Kutta method from [37], the time response is illustrated in Figure 9. As observed, the response obtained using the analytical method aligns closely with the response produced by the numerical method, demonstrating strong agreement between the two approaches. The convergence of the response to zero over time indicates that, for the given parameters, the MNVA effectively reduces the vibrations in the rotor system, leading to system stabilization. This close match confirms the reliability of the multiple time scales method in predicting the dynamic behavior of the system.
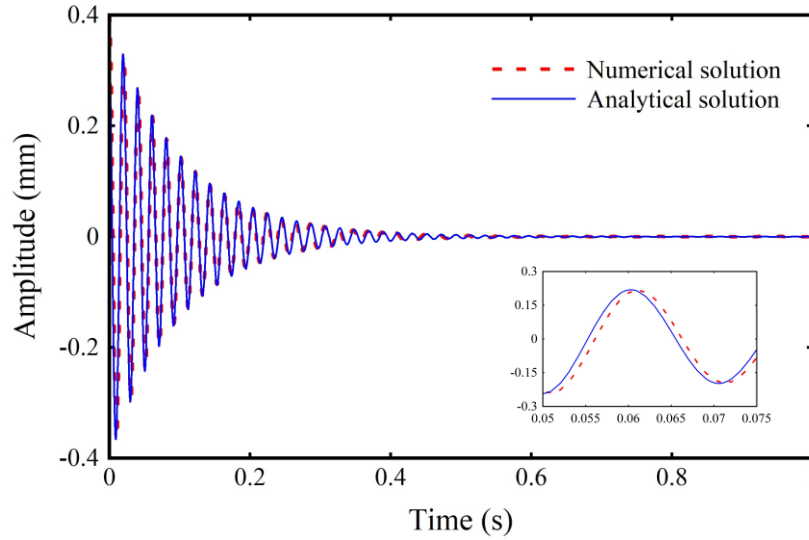
Figure 9: Comparison of the analytical and numerical solutions of the rotor system's equations equipped with a MNVA

To assess the advantages of using a MNVA over a linear vibration absorber (LVA), Figure 10 presents the time response of the rotor system equipped with both types of absorbers, starting from an initial displacement of 0.4 mm. The results show that when the LVA is connected, the oscillation amplitude takes approximately 0.32 seconds to reduce to 0.047 mm. In contrast, with the MNVA attached, the amplitude decreases to the same value in about 0.2 seconds. This indicates that the vibration absorption speed of the MNVA is 1.6 times faster than that of the LVA. The enhanced performance of the MNVA highlights its superior ability to more rapidly mitigate vibrations, providing a more efficient solution for vibration control in rotor systems.
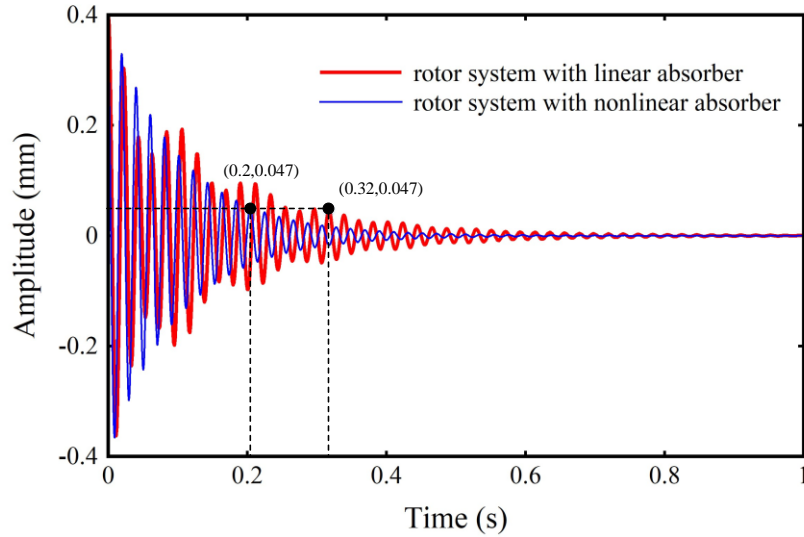
Figure 10: Comparison of the time response of the rotor system equipped with a LVA and a MNVA

Figure 11 illustrates the frequency response curves of the rotor system equipped with both the MNVA and the LVA. The maximum amplitude for the rotor system with the LVA is observed to be 0.027 mm, whereas the maximum amplitude with the MNVA is reduced to 0.022 mm. This difference highlights that the MNVA achieves approximately a 22% greater reduction in vibration amplitude compared to the LVA. Therefore, it can be concluded that the MNVA is more effective in minimizing rotor system vibrations, providing a significant improvement in vibration control performance over the LVA.
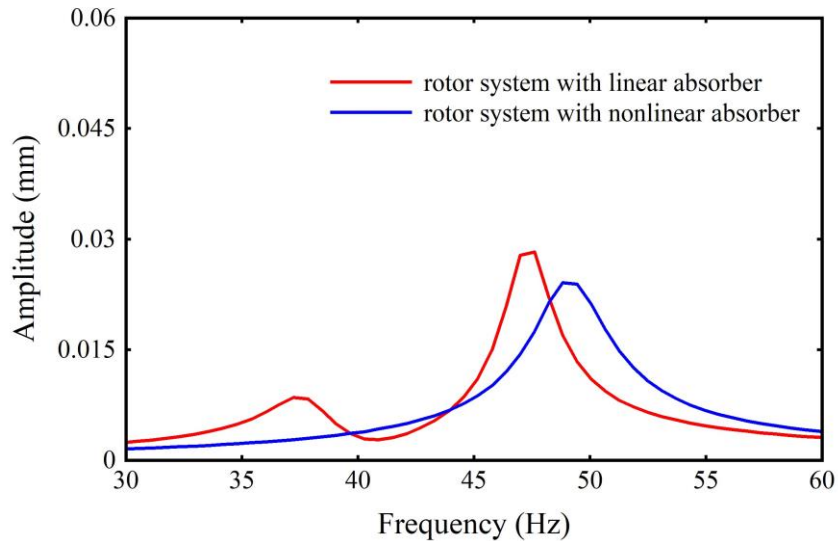
Figure 11: Comparison of the frequency response of the rotor system equipped with LVA and a MNVA

4. Conclusions

In previous research, the dynamic behavior of rotor systems equipped with a multi-stable nonlinear vibration absorber (MNVA) has predominantly been explored using numerical methods. While numerical methods are efficient for generating time and frequency responses for specific parameter values, they require recalculating the solution for each new parameter to assess its impact on the system's behavior. Semi-analytical methods, on the other hand, provide an advantage by allowing the effects of various linear and nonlinear parameters to be examined more easily without the need for repeated recalculations. Although these methods can increase computational demands, they are often preferred for their broader applicability.

In this study, for the first time, the response of a rotor system equipped with a MNVA was derived using the perturbation method of multiple scales with a first-order approximation. The effects of different system parameters on the response were investigated. The results obtained from the multiple scales method were validated through comparison with numerical solutions generated using the Runge-Kutta method as described in Ref. [37]. Additionally, the advantages of using a MNVA over a linear vibration absorber (LVA) were evaluated. The findings demonstrate that the multiple scales method provides highly accurate results in both short- and long-term intervals. The key conclusions of this study are as follows:

1. To reduce the maximum oscillation amplitude of the rotor system equipped with a MNVA, the stiffness of both the primary rotor system and the absorber as well as the primary system's damping should be increased, while the rotor's centrifugal force should be reduced.

2. Increasing the total bending stiffness of the absorber rods significantly shifts the frequency response curve away from resonance, enhancing the system stability.

3. Positive changes in the nonlinear stiffness of the absorber spring shift the frequency response curve to the left, while negative changes shift it to the right. These shifts create a three-response region or jump phenomenon, although the system's maximum amplitude remains unaffected.

4. Variations in the vibration absorber's damping coefficient do not impact the oscillation amplitude of the rotor system equipped with a MNVA.

5. The vibration absorption efficiency of the MNVA is 22% higher than that of the LVA, demonstrating its superior performance in reducing rotor system vibrations.

Finally, the comparison of the responses obtained from the analytical and numerical methods shows that they are nearly coincident, with no significant differences between them, validating the accuracy of the proposed semi-analytical approach.

References

[1]   Zhou P, Chen S, He Q, Wang D, Peng Z. Rotating machinery fault-induced vibration signal modulation effects: A review with mechanisms, extraction methods and applications for diagnosis. Mechanical Systems and Signal Processing. 2023;200:110489.

[2]   Wu T, Zhang W, Zhang B, Luo H. Application of multi-base fusion generalized chirplet basis transform in vibration signal analysis of multiple rotor rotating machinery. Mechanical Systems and Signal Processing. 2023;185:109792.

[3] Mishra RK, Choudhary A, Fatima S, Mohanty AR, Panigrahi BK. A generalized method for diagnosing multi-faults in rotating machines using imbalance datasets of different sensor modalities. Engineering Applications of Artificial Intelligence. 2024;132:107973.

[4] Tama BA, Vania M, Lee S, Lim S. Recent advances in the application of deep learning for fault diagnosis of rotating machinery using vibration signals. Artificial Intelligence Review. 2023;56(5):4667-709.

[5] Romanssini M, de Aguirre PCC, Compassi-Severo L, Girardi AG. A review on vibration monitoring techniques for predictive maintenance of rotating machinery. Eng. 2023;4(3):1797-817.

[6] Fan L, Inoue T, Heya A, Watanabe Y. Predicting stability of synchronous nonlinear vibration in vertical rotating shaft system with journal bearing. Journal of Sound and Vibration. 2024;572:118191.

[7] Yao B, Tian Z, Zhan X, Li C, Yu H. Study on Rotor-Bearing System Vibration of Downhole Turbine Generator under Drill-String Excitation. Energies. 2024;17(5):1176.

[8] Tselios I, Nikolakopoulos P. Identification of Unbalance in a Rotating System Using Artificial Neural Networks. Olympiad in Engineering Science: Springer; 2023. p. 311-26.

[9] Matania O, Bachar L, Bechhoefer E, Bortman J. Signal processing for the condition-based maintenance of rotating machines via vibration analysis: A tutorial. Sensors. 2024;24(2):454.

[10] Wang Z, Hu H, Yang J, Zheng J, Zhao W, Ouyang Q. Experimental Study on the Skyhook Control of a Magnetorheological Torsional Vibration Damper. Micromachines. 2024;15(2):236.

[11] Chowdhury S, Banerjee A. The impacting vibration absorbers. Applied Mathematical Modelling. 2024;127:454-505.

[12] Huang X, Yang B. Towards novel energy shunt inspired vibration suppression techniques: principles, designs and applications. Mechanical Systems and Signal Processing. 2023;182:109496.

[13] Jiao X, Zhang J, Li W, Wang Y, Ma W, Zhao Y. Advances in spacecraft micro-vibration suppression methods. Progress in Aerospace Sciences. 2023;138:100898.

[14] Li D, Ikago K, Yin A. Structural dynamic vibration absorber using a tuned inerter eddy current damper. Mechanical Systems and Signal Processing. 2023;186:109915.

[15] Watts P. On a method of reducing the rolling of ships at sea. Read at the 24th Session of the Royal Institution of Naval Architects, RINA Transactions: 1883-12, March 16, 1883. 1883.

[16] Frahm H. Device for damping vibrations of bodies. Google Patents; 1911.

[17] Doubrawa Filho F, Luersen M, Bavastri C. Optimal design of viscoelastic vibration absorbers for rotating systems. Journal of Vibration and Control. 2011;17(5):699-710.

[18] Hu W, Li S, Yang M, Ding M, Yu Y, editors. Numerical simulation of helicopter rotor blade vertical pendulum absorbers. Journal of Physics: Conference Series; 2024: IOP Publishing.

[19] Hu H-l, He L-d. Online control of critical speed vibrations of a single-span rotor by a rotor dynamic vibration absorber at different installation positions. Journal of Mechanical Science and Technology. 2017;31:2075-81.

[20] Ouyang X, Cao S, Li G. Nonlinear dynamics of a dual-rotor-bearing system with active elastic support dry friction dampers. Nonlinear Dynamics. 2024;112(10):7875-907.

[21] Gendelman O, Starosvetsky Y, Feldman M. Attractors of harmonically forced linear oscillator with attached nonlinear energy sink I: description of response regimes. Nonlinear Dynamics. 2008;51:31-46.

[22] Starosvetsky Y, Gendelman OV. Attractors of harmonically forced linear oscillator with attached nonlinear energy sink. II: optimization of a nonlinear vibration absorber. Nonlinear Dynamics. 2008;51:47-57.

[23] Ma K, Du J, Zhang H, Liu Y, Chen X. A comparative study on the torsional vibration suppression of rotor system using variable steady state nonlinear energy sink. Chaos, Solitons & Fractals. 2024;185:115144.

[24] Kumar RK, Kumar N. Multi-mode vibration suppression of a cantilever beam carrying unbalance rotor using bi-stable nonlinear energy sink. Noise & Vibration Worldwide. 2024:09574565241278719.

[25] Yang K, Zhang Y-W, Ding H, Yang T-Z, Li Y, Chen L-Q. Nonlinear energy sink for whole-spacecraft vibration reduction. Journal of Vibration and Acoustics. 2017;139(2):021011.

[26] Bab S, Khadem S, Shahgholi M, Abbasi A. Vibration attenuation of a continuous rotor-blisk-journal bearing system employing smooth nonlinear energy sinks. Mechanical Systems and Signal Processing. 2017;84:128-57.

[27] Gzal MO, Gendelman OV, Bergman LA, Vakakis AF. Enhanced seismic mitigation through energy management using nonlinear energy sinks with clearance–contacts. Nonlinear Dynamics. 2024:1-22.

[28] Bergeot B, Bellizzi S, Cochelin B. Passive suppression of helicopter ground resonance using nonlinear energy sinks attached on the helicopter blades. Journal of Sound and Vibration. 2017;392:41-55.

[29] Yao H, Wang Y, Xie L, Wen B. Bi-stable buckled beam nonlinear energy sink applied to rotor system. Mechanical Systems and Signal Processing. 2020;138:106546.

[30] Abu Seer T, Vahdati N, Shiryayev O. Adaptive torsional tuned vibration absorber for rotary equipment. Vibration. 2019;2(1):116-34.

[31] Yao H, Chen Z, Wen B. Dynamic vibration absorber with negative stiffness for rotor system. Shock and Vibration. 2016;2016(1):5231704.

[32] Dong X, Li W, Yu J, Pan C, Xi J, Zhou Y, et al. Magneto-rheological variable stiffness and damping torsional vibration control of powertrain system. Frontiers in Materials. 2020;7:121.

[33] Yao H, Wang Y, Cao Y, Wen B. Multi-stable nonlinear energy sink for rotor system. International Journal of Non-Linear Mechanics. 2020;118:103273.

[34] Cao Y, Yao H, Li Q, Yang P, Wen B. Vibration mitigation and dynamics of a rotor-blade system with an attached nonlinear energy sink. International Journal of Non-Linear Mechanics. 2020;127:103614.

[35] Yao H, Wang T, Wen B, Qiu B. A tunable dynamic vibration absorber for unbalanced rotor system. Journal of Mechanical Science and Technology. 2018;32:1519-28.

[36] Gao P, Liu H, Xiang C, Yan P, Mahmoud T. A new magnetorheological elastomer torsional vibration absorber: structural design and performance test. Mechanical Sciences. 2021;12(1):321-32.

[37] Yao H, Cao Y, Ding Z, Wen B. Using grounded nonlinear energy sinks to suppress lateral vibration in rotor systems. Mechanical systems and signal processing. 2019;124:237-53.

[38] Nayfeh AH, Mook DT. Nonlinear oscillations: John Wiley & Sons; 2008.